Effect of uniaxial and biaxial crystal-field potential on magnetic properties of a mixed spin-1/2 and spin-1 Ising model on honeycomb lattice

Jozef Strečka and Michal Jaščur

Department of Theoretical Physics and Astrophysics, Institute of Physics,
P. J. Šafárik University, Park Angelinum 9, 040 01 Košice, Slovak Republic

E-mail: jozkos@pobox.sk, jascur@kosice.upjs.sk

(Submitted:February 2, 2008)

Magnetic properties of a mixed spin-1/2 and spin-1 Ising model on honeycomb lattice are exactly investigated within the framework of generalized star-triangle mapping transformation. The particular attention is focused on the effect of uniaxial and biaxial crystal-field anisotropies that basically influence the magnetic behaviour of the spin-1 atoms. Our results for the basic thermodynamic quantities, as well as the dynamical time-dependent autocorrelation function indicate the spin tunneling between the $|+1\rangle$ and $|-1\rangle$ states in the magnetically ordered phase.

Keywords: uniaxial and biaxial crystal-field anisotropy; exact solution; star-triangle transformation
PACS: 75.10.Hk, 05.50.+q

I. INTRODUCTION

Over the last few years, many non-trivial quantum phenomena have been discovered in the low-dimensional magnetic materials. One of the most actively studied problems in the condensed matter physics at present is a quantum tunneling of magnetization, i. e. the effect, which has been recently developed in a large number of single-molecule magnets (see Ref. [1] and references therein). By the term single-molecule magnets, one denotes the small clusters of magnetic metal ions that usually possess an extraordinary strong magnetic anisotropy. Hence, the single-molecule magnets often provide very good examples of so-called Ising-like spin systems with a strong uniaxial magnetic anisotropy. Of course, the Ising anisotropy by itself cannot be a source of the quantum spin tunneling experimentally observed in these systems. It turns out, however, that this quantum phenomenon arises in the most cases due to the higher-order crystal-field terms. According to a number of experimental and theoretical studies it is now quite well established, that the observed spin tunneling originates to a major extent from the second-order biaxial crystal-field potential, at least in Fe_4[2], Fe_8[3], Fe_{19}[4], or Mn_4[5] compounds.

The immense interest in the magnetic properties of small magnetic clusters shed light on the effect of single-ion anisotropy terms D (uniaxial anisotropy) and E (biaxial, also called rhombic anisotropy). In contrast to the quite well understood role of the both single-ion anisotropies D and E in the small magnetic clusters (zero-dimensional systems), the situation is much more complicated and also obscure in one- and two-dimensional spin systems. In fact, the ground-state properties of a spin-S Ising model with the

rhombic crystal-field potential E, have been only recently examined by Oitmaa and von Brasch within an effective mapping to the transverse Ising model[6]. On the basis of this effective mapping, the $T = 0$ quantum critical point can be exactly located for the one-dimensional model, while for the two-dimensional models they can be obtained with a high numerical accuracy using the linked-cluster expansion method[6,7]. Nevertheless, the finite temperature behaviour of these models has not been investigated in detail beyond the standard mean-field and effective-field theories[8], random phase approximation[9], or linked cluster expansion[10]. It should be stressed that the biaxial anisotropy essentially influences the magnetic properties of a large number of polymeric molecular-based magnetic materials, too. From the most obvious examples one could mention: NiF_2[11], $NiNO_3.6H_2O$[12], $Ni(CH_3COO)_2.4H_2O$[13], $Mn(CH_3COO)_2.3H_2O$[14], CoF_2[15], $CoCl_2.6H_2O$[16] and a series of compounds $Fe(dc)_2X$[17], where X stands for halids and dc for the dithiocarbamate or diselenocarbamate groups, respectively.

Owing to this fact, in this article we will focus on the uniaxial and biaxial crystal-field anisotropies affecting the magnetic behaviour of the mixed spin-1/2 and spin-1 honeycomb lattice. By assuming an Ising-type exchange interaction between the nearest-neighbouring spins, the model under investigation can be exactly treated through the generalized star-triangle mapping transformation. The considered model thus provides a noble example of the statistical system, which enables to study an interplay between quantum effects and temperature in a spontaneously ordered magnetic system. Moreover, the magnetic structure of a mixed-spin honeycomb lattice occurs rather frequently also in the molecular magnetism, what clearly demonstrates a large family of polymeric two-dimensional compounds of chemical formula: $A^{I}M^{II}M^{III}(C_2O_4)_3$[18], where A^{I} stands for a non-magnetic univalent cation $N(C_nH_{2n+1})_4$ or $P(C_nH_{2n+1})_4$ ($n = 3 - 5$), M^{II} and M^{III} denote two- and three-valent metal atoms $Cu^{II}(S = 1/2)$, $Ni^{II}(S = 1)$, $Co^{II}(S = 3/2)$, $Fe^{II}(S = 2)$ or $Mn^{II}(S = 5/2)$ and $Cr^{III}(S = 3/2)$ or $Fe^{III}(S = 5/2)$, respectively. Indeed, the crystal structure of these polymeric molecular-based magnetic materials consists of the well-separated two-dimensional layers in which regularly alternating M^{II} and M^{III} magnetic metal atoms constitute more or less regular honeycomb lattice (Fig. 1). As a consequence of the anisotropic crystalline structure of these materials, one should also expect a relatively strong uniaxial (Ising-like) anisotropy, as it has already been suggested in the theoretical studies based on the effective-field theory and Monte-Carlo simulations[19]. Hence, the magnetic compounds from the family of oxalates $A^{I}M^{II}M^{III}(C_2O_4)_3$ represent good candidates to be described by the proposed model.

The outline of this paper is as follows. In the next section the detailed description of the model system will be presented and then, some basic aspects of the transformation method will be shown. Section 3 deals with the physical interpretation of the most interesting results and finally, some concluding remarks are drawn in Section 4.

II. MODEL AND METHOD

Let us consider the magnetic structure of a mixed-spin honeycomb lattice schematically depicted in Fig. 1. To ensure exact solvability of the model under investigation, we will further suppose that the sites

of sublattice A are occupied by the spin-1/2 atoms (depicted as full circles), in contrast to the sites of sublattice B that are occupied by the spin-1 atoms (open circles). By assuming the Ising-type exchange interaction J between nearest-neighbouring spins, the total Hamiltonian of the system takes the following form:

$$\hat{\mathcal{H}} = J \sum_{\langle k,j \rangle}^{3N} \hat{S}_k^z \hat{\mu}_j^z + D \sum_{k \in B}^{N} (\hat{S}_k^z)^2 + E \sum_{k \in B}^{N} [(\hat{S}_k^x)^2 - (\hat{S}_k^y)^2], \tag{1}$$

where N is a total number of sites at each sublattice, $\hat{\mu}_j^z$ and $\hat{S}_k^\alpha (\alpha = x, y, z)$ denote the standard spatial components of the spin-1/2 and spin-1 operators, respectively. The first summation in Eq. (1) is carried out over the nearest-neighbouring spin pairs, while the other two summations run over the sites of sublattice B. Apparently, the last two terms D and E are the crystal-field potentials that measure a strength of the uniaxial and biaxial anisotropy acting on the spin-1 atoms. It is also worth noticing that there is one-to-one correspondence between the Hamiltonian (1) and the effective spin Hamiltonian with three different single-ion anisotropies D^x, D^y and D^z:

$$\hat{\mathcal{H}} = J \sum_{\langle k,j \rangle}^{3N} \hat{S}_k^z \hat{\mu}_j^z + D^z \sum_{k \in B}^{N} (\hat{S}_k^z)^2 + D^x \sum_{k \in B}^{N} (\hat{S}_k^x)^2 + D^y \sum_{k \in B}^{N} (\hat{S}_k^y)^2. \tag{2}$$

In fact, one can easily prove the equivalence between the two effective spin Hamiltonians (up to the unimportant additive constant, for a comparison see[20]), which can be achieved using this simple mapping between the relevant parameters included in the Hamiltonians (1) and (2), respectively:

$$D = D^z - \frac{1}{2}(D^x + D^y), \qquad \text{and} \qquad E = \frac{1}{2}(D^x - D^y). \tag{3}$$

It should be also mentioned here that by neglecting the biaxial anisotropy, i. e. setting $E = 0$ in Eq. (1) or equivalently $D^x = D^y$ in Eq. (2), our model reduces to the exactly soluble model of Gonçalves[21]. Accordingly, in this work we will in particular examine the effect of biaxial anisotropy on the thermodynamical and dynamical properties of the model under consideration. Nevertheless, the E term emerging in the Hamiltonian (1) should cause non-trivial quantum effects, since it introduces the x and y components of spin operators into the Hamiltonian and thus, it is responsible for the onset of local quantum fluctuations that are obviously missing in the Ising model with the uniaxial crystal-field potential D only.

It is therefore of interest to discuss the origin of biaxial anisotropy. The origin of this anisotropy term consists in the low-symmetry crystal field of ligands from the local neighbourhood of spin-1 atoms. A threefold symmetry axis oriented perpendicular to the honeycomb layer, however, prevents the appearance of biaxial crystal-field potential in a regular honeycomb lattice with a perfect arrangement of the oxalato groups, as well as magnetic metal atoms. On the other hand, the small lattice distortion, which occurs rather frequently in the low-dimensional polymeric compounds due to the Jahn-Teller effect, can potentially lower the local symmetry. In consequence of that, the distortion of lattice parameters can be regarded as a possible source of the biaxial anisotropy. The most obvious example, where the lattice distortion removes the threefold symmetry axis represents the single-molecule magnet Fe_4, in which three outer Fe atoms occupy two non-equivalent positions around one central Fe atom[2].

Let us turn our attention to the main points of the transformation method, which enables an exact treatment of the model under investigation. Firstly, it is very convenient to write the total Hamiltonian (1) as a sum of the site Hamiltonians $\hat{\mathcal{H}}_k$:

$$\hat{\mathcal{H}} = \sum_{k\in B}^{N} \hat{\mathcal{H}}_k, \tag{4}$$

where each site Hamiltonian $\hat{\mathcal{H}}_k$ involves all interaction terms associated with the appropriate spin-1 atom residing on the kth site of sublattice B:

$$\hat{\mathcal{H}}_k = \hat{S}_k^z E_k + (\hat{S}_k^z)^2 D + [(\hat{S}_k^x)^2 - (\hat{S}_k^y)^2]E, \tag{5}$$

with $E_k = J(\hat{\mu}_{k1}^z + \hat{\mu}_{k2}^z + \hat{\mu}_{k3}^z)$. While the Hamiltonians (5) at different sites commute with each other ($[\hat{\mathcal{H}}_i, \hat{\mathcal{H}}_j] = 0$, for each $i \neq j$), the partition function of the system can be partially factorized and consequently, rewritten in the form:

$$\mathcal{Z} = \mathrm{Tr}_{\{\mu\}} \prod_{k=1}^{N} \mathrm{Tr}_{S_k} \exp(-\beta\hat{\mathcal{H}}_k). \tag{6}$$

In above, $\beta = 1/(k_B T)$, k_B is Boltzmann's constant, T the absolute temperature, $\mathrm{Tr}_{\{\mu\}}$ means a trace over the spin degrees of freedom of sublattice A and Tr_{S_k} stands for a trace over the spin states of kth spin from sublattice B. So, a crucial step in our procedure represents the calculation of the expression $\mathrm{Tr}_{S_k} \exp(-\beta\hat{\mathcal{H}}_k)$. With regard to this, let us write the site Hamiltonian (5) in an usual matrix representation:

$$\hat{\mathcal{H}}_k = \begin{pmatrix} D + E_k & 0 & E \\ 0 & 0 & 0 \\ E & 0 & D - E_k \end{pmatrix}, \tag{7}$$

in a standard basis of functions $|\pm 1\rangle, |0\rangle$ corresponding, respectively, to the three possible spin states $S_k^z = \pm 1, 0$ of kth atom from sublattice B. Obviously, it is easy to find eigenvalues of the site Hamiltonian (7), however, with respect to further calculation, it is more favourable to obtain directly the matrix elements of the expression $\exp(-\beta\hat{\mathcal{H}}_k)$. Using the well-known Cauchy integral formula, one readily obtains the matrix elements for an arbitrary exponential function of the site Hamiltonian (7):

$$\exp(\alpha\hat{\mathcal{H}}_k) = \exp(\alpha D) \begin{pmatrix} \cosh(\alpha\Theta) + \frac{E_k}{\Theta}\sinh(\alpha\Theta) & 0 & \frac{E}{\Theta}\sinh(\alpha\Theta) \\ 0 & \exp(-\alpha D) & 0 \\ \frac{E}{\Theta}\sinh(\alpha\Theta) & 0 & \cosh(\alpha\Theta) - \frac{E_k}{\Theta}\sinh(\alpha\Theta) \end{pmatrix}, \tag{8}$$

where $\Theta = \sqrt{E_k^2 + E^2}$ and α marks any multiplicative function. After substituting $\alpha = -\beta$ into the Eq. (8), the calculation of the relevant trace $\mathrm{Tr}_{S_k} \exp(-\beta\hat{\mathcal{H}}_k)$ can be accomplished, moreover, its explicit form immediately implies a possibility of performing a standard star-triangle mapping transformation:

$$\begin{aligned} \mathrm{Tr}_{S_k} \exp(-\beta\hat{\mathcal{H}}_k) &= 1 + 2\exp(-\beta D)\cosh\Big(\beta\sqrt{J^2(\mu_{k1}^z + \mu_{k2}^z + \mu_{k3}^z)^2 + E^2}\Big) = \\ &= A\ \exp\Big[\beta R(\mu_{k1}^z\mu_{k2}^z + \mu_{k2}^z\mu_{k3}^z + \mu_{k3}^z\mu_{k1}^z)\Big], \end{aligned} \tag{9}$$

which replaces the partition function of a *star*, i. e. the four-spin cluster consisting of one central spin-1 atom and its three nearest-neighbouring spin-1/2 atoms, by the partition function of a *triangle*, i. e. the three-spin cluster comprising of three spin-1/2 atoms in the corners of equilateral triangle (see Fig. 1). The physical meaning of the mapping (9) is to remove all interaction parameters associated with the central spin-1 atom and to replace them by an effective interaction R between the outer spin-1/2 atoms. It is noteworthy, that the both mapping parameters A and R are "self-consistently" given by the transformation equation (9), which must be valid for any combination of spin states of three spin-1/2 atoms. In consequence of that one obtains:

$$A = \Big(\Phi_1\Phi_2^3\Big)^{1/4}, \qquad\qquad \beta R = \ln\Big(\frac{\Phi_1}{\Phi_2}\Big), \tag{10}$$

where we have introduced the functions Φ_1 and Φ_2 to write the transformation parameters (10) in more abbreviated and elegant form:

$$\begin{aligned}\Phi_1 &= 1 + 2\exp(-\beta D)\cosh\Big(\beta\sqrt{(3J/2)^2 + E^2}\Big),\\ \Phi_2 &= 1 + 2\exp(-\beta D)\cosh\Big(\beta\sqrt{(J/2)^2 + E^2}\Big).\end{aligned} \tag{11}$$

When the mapping (9) is performed at each site of the sublattice B, the original mixed-spin honeycomb lattice is mapped onto the spin-1/2 triangular lattice with the effective interaction R given by the "self-consistency" condition (10)-(11). As a matter of fact, the substitution of the mapping transformation (9) into the partition function (6) establishes the relationship:

$$\mathcal{Z}(\beta, J, D, E) = A^N \mathcal{Z}_t(\beta, R), \tag{12}$$

between the partition function $\mathcal{Z}$ of the mixed-spin honeycomb lattice and the partition function $\mathcal{Z}_t$ of the corresponding spin-1/2 triangular lattice. Above equation constitutes the basic result of our calculation, since it enables relatively simple derivation of all required quantities such as magnetization, quadrupolar moment, correlation function, internal energy, specific heat, etc. Moreover, by combining (12) with (9) one easily proves the validity of following exact spin identities:

$$\begin{aligned}\langle f_1(\mu_i^z, \mu_j^z, ..., \mu_k^z)\rangle &= \langle f_1(\mu_i^z, \mu_j^z, ..., \mu_k^z)\rangle_t,\\ \langle f_2(S_k^x, S_k^y, S_k^z, \mu_{k1}^z, \mu_{k2}^z, \mu_{k3}^z)\rangle &= \left\langle \frac{\mathrm{Tr}_{S_k} f_2(S_k^x, S_k^y, S_k^z, \mu_{k1}^z, \mu_{k2}^z, \mu_{k3}^z)\exp(-\beta\hat{\mathcal{H}}_k)}{\mathrm{Tr}_{S_k}\exp(-\beta\hat{\mathcal{H}}_k)}\right\rangle,\end{aligned} \tag{13}$$

where $\langle ...\rangle$ represents the standard canonical average over the ensemble defined by the Hamiltonian (1) and $\langle ...\rangle_t$ canonical average performed on the spin-1/2 Ising triangular lattice with the effective exchange interaction R (10)-(11). Furthermore, f_1 is an arbitrary function of the spin variables belonging to the sublattice A, while f_2 denotes an arbitrary function depending on the kth spin from sublattice B and its three nearest-neighbours from sublattice A. Applying the first of spin identities (13), one straightforwardly attains the following results:

$$m_A \equiv \langle\hat{\mu}_{k1}^z\rangle = \langle\hat{\mu}_{k1}^z\rangle_t \equiv m_t, \tag{14}$$

$$c_A \equiv \langle\hat{\mu}_{k1}^z\hat{\mu}_{k2}^z\rangle = \langle\hat{\mu}_{k1}^z\hat{\mu}_{k2}^z\rangle_t \equiv c_t, \tag{15}$$

$$t_A \equiv \langle\hat{\mu}_{k1}^z\hat{\mu}_{k2}^z\hat{\mu}_{k3}^z\rangle = \langle\hat{\mu}_{k1}^z\hat{\mu}_{k2}^z\hat{\mu}_{k3}^z\rangle_t \equiv t_t, \tag{16}$$

while the second of spin identities (13) enables a derivation of quantities depending on the spin variable from sublattice B, as well:

$$m_B \equiv \langle \hat{S}_k^z \rangle = -3m_A(K_1+K_2)/2 - 2t_A(K_1-3K_2), \tag{17}$$

$$q_B^x \equiv \langle (\hat{S}_k^x)^2 \rangle = (K_5+3K_6)/4 + 3c_A(K_5-K_6), \tag{18}$$

$$q_B^y \equiv \langle (\hat{S}_k^y)^2 \rangle = (K_7+3K_8)/4 + 3c_A(K_7-K_8), \tag{19}$$

$$q_B^z \equiv \langle (\hat{S}_k^z)^2 \rangle = (K_3+3K_4)/4 + 3c_A(K_3-K_4). \tag{20}$$

In above, m_A (m_B) labels the single-site magnetization at sublattice A (B), $q_B^\alpha (\alpha = x,y,z)$ are different spatial components of quadrupolar moment and finally, c_A and t_A static pair and triplet correlation functions between the relevant spins of sublattice A, respectively. Obviously, an exact solution for the both sublattice magnetization and quadrupolar moment require the knowledge of the single-site magnetization m_t, nearest-neighbour pair correlation function c_t and triplet correlation function t_t on the corresponding spin-1/2 triangular lattice unambiguously given by (10)-(11). Fortunately, the exact solution for these quantities on spin-1/2 triangular lattice are known long time ago, hence, one can utilize the final results from references[22]. Finally, the coefficients emerging in the previous set of Eqs. (17)-(20) are listed below:

$$\begin{aligned} &K_1 = F_1(3J/2), \qquad K_2 = F_1(J/2), \qquad K_3 = F_2(3J/2), \qquad K_4 = F_2(J/2), \\ &K_5 = F_3(3J/2,-E), \quad K_6 = F_3(J/2,-E), \quad K_7 = F_3(3J/2,E), \quad K_8 = F_3(J/2,E), \end{aligned} \tag{21}$$

where we have defined the functions $F_1(x)$, $F_2(x)$ and $F_3(x,y)$ as follows:

$$\begin{aligned} F_1(x) &= \frac{x}{\sqrt{x^2+E^2}} \frac{2\sinh(\beta\sqrt{x^2+E^2})}{\exp(\beta D) + 2\cosh(\beta\sqrt{x^2+E^2})}; \\ F_2(x) &= \frac{2\cosh(\beta\sqrt{x^2+E^2})}{\exp(\beta D) + 2\cosh(\beta\sqrt{x^2+E^2})}; \\ F_3(x,y) &= \frac{\exp(\beta D) + \cosh(\beta\sqrt{x^2+y^2})}{\exp(\beta D) + 2\cosh(\beta\sqrt{x^2+y^2})} + \frac{y}{\sqrt{x^2+y^2}} \frac{\sinh(\beta\sqrt{x^2+y^2})}{\exp(\beta D) + 2\cosh(\beta\sqrt{x^2+y^2})}. \end{aligned} \tag{22}$$

At the end of this section, we will also provide an exact result for one dynamical quantity - time-dependent autocorrelation function. It should be noted here that the exactly soluble models offer only seldom the possibility to investigate their spin dynamics. On the other hand, the dynamical quantities such as autocorrelation and correlation functions are important also from the experimental point of view, because their magnitude directly determines the scattering cross section measured in the inelastic neutron scattering experiments[23], or the spin-lattice relaxation rate provided by the nuclear magnetic resonance (NMR) techniques[24]. In this work, an exact treatment for the time-dependent autocorrelation function will be elaborated. As a starting point for the calculation of the autocorrelation function $C_{auto}^{zz}(t)$ can for convenience serve the second of exact spin identities (13):

$$\begin{aligned} C_{auto}^{zz}(t) &\equiv \frac{1}{2}\langle \hat{S}_k^z(0)\hat{S}_k^z(t) + \hat{S}_k^z(t)\hat{S}_k^z(0) \rangle = \\ &= \frac{1}{2}\Big\langle \frac{\mathrm{Tr}_{S_k}\{[\hat{S}_k^z(0)\hat{S}_k^z(t) + \hat{S}_k^z(t)\hat{S}_k^z(0)]\exp(-\beta\hat{\mathcal{H}}_k)\}}{\mathrm{Tr}_{S_k}\exp(-\beta\hat{\mathcal{H}}_k)} \Big\rangle, \end{aligned} \tag{23}$$

where the symmetrized form in the definition of C^{zz}_{auto} is used to construct a hermitian operator, $\hat{S}^z_k(t) = \exp(\frac{it\hat{\mathcal{H}}_k}{\hbar})\hat{S}^z_k \exp(-\frac{it\hat{\mathcal{H}}_k}{\hbar})$ represents the Heisenberg picture for the time-dependent operator $\hat{S}^z_k(t)$, $\hbar$ stands for Planck's constant and $i = \sqrt{-1}$. Next, the matrix representation of $\exp(\pm\frac{it\hat{\mathcal{H}}_k}{\hbar})$ can be readily obtained by putting $\alpha = \pm\frac{it}{\hbar}$ into Eq. (8). Then, after straightforward but a little bit tedious calculation, one arrives to the final result for the dynamical autocorrelation function:

$$C^{zz}_{auto}(t) = K_3\Big(\frac{1}{4} + 3c_t\Big)\frac{(\frac{3}{2}J)^2 + E^2\cos\Big(\frac{2t}{\hbar}\sqrt{(\frac{3}{2}J)^2 + E^2}\Big)}{(\frac{3}{2}J)^2 + E^2} + \\ + K_4\Big(\frac{3}{4} - 3c_t\Big)\frac{(\frac{1}{2}J)^2 + E^2\cos\Big(\frac{2t}{\hbar}\sqrt{(\frac{1}{2}J)^2 + E^2}\Big)}{(\frac{1}{2}J)^2 + E^2}. \tag{24}$$

III. RESULTS AND DISCUSSION

Before proceeding to the discussion of the most interesting results, it is noteworthy, that the results derived in the previous section are rather general, i. e. they are valid for the ferromagnetic ($J < 0$), as well as ferrimagnetic ($J > 0$) version of the model under consideration. In what follows, we will restrict ourselves to the analysis of the ferrimagnetic model only, since the polymeric compounds from the family of oxalates[18] fall mostly into the class of ferrimagnets. Nevertheless, it appears worthwhile to say that magnetic behaviour of the ferrimagnetic system completely resembles that one of the ferromagnetic system. Finally, it should be emphasized that the mapping (9) remains invariant under the transformation $E \leftrightarrow -E$. As a result, one may consider without loss of generality the parameter $E \geq 0$ and consequently, x-, y- and z-axis then represent the hard-, medium- and easy-axis for a given system.

A. Ground-state properties

At first, we will take a closer look at the ground-state behaviour. Taking into account the zero-temperature limit $T \to 0^+$, one finds following condition for a first-order phase transition line separating the magnetically ordered phase (OP) from the disordered phase (DP):

$$\frac{D}{J} = \sqrt{\Big(\frac{3}{2}\Big)^2 + \Big(\frac{E}{J}\Big)^2}. \tag{25}$$

From Eqs. (16)-(22), moreover, one easily attains analytical results for the single-site sublattice magnetization (m_A, m_B), total single-site magnetization $m = (m_A + m_B)/2$ and different spatial components of the quadrupolar moment $q^\alpha_B(\alpha = x, y, z)$ in the both phases, as well:

$$\text{OP:} \qquad m_A = -\frac{1}{2}, \qquad m_B = \frac{\frac{3}{2}}{\sqrt{\Big(\frac{3}{2}\Big)^2 + \Big(\frac{E}{J}\Big)^2}}, \qquad m = -\frac{1}{4} + \frac{\frac{3}{4}}{\sqrt{\Big(\frac{3}{2}\Big)^2 + \Big(\frac{E}{J}\Big)^2}}, \\ q^x_B = \frac{1}{2}\Big(1 - \frac{\frac{E}{J}}{\sqrt{(\frac{3}{2})^2 + (\frac{E}{J})^2}}\Big), \quad q^y_B = \frac{1}{2}\Big(1 + \frac{\frac{E}{J}}{\sqrt{(\frac{3}{2})^2 + (\frac{E}{J})^2}}\Big), \quad q^z_B = 1.0; \tag{26}$$

$$\text{DP}: \quad m_A{=}0.0, \quad m_B = 0.0, \quad m = 0.0,$$
$$q_B^x{=}1.0, \quad q_B^y = 1.0, \quad q_B^z = 0.0. \tag{27}$$

For better illustration, Fig. 2 depicts the ground-state phase diagram in the E/J-D/J plane (Fig. 2a) together with the zero-temperature variations of the magnetization and quadrupolar moment in the OP (Fig. 2b, the value of uniaxial anisotropy $D/J = 0.0$ has been chosen not to pass through the phase boundary). It is worthy to mention that by neglecting the biaxial anisotropy, i. e. setting $E/J = 0.0$, one recovers from the phase boundary condition (25) a boundary uniaxial anisotropy $D/J = 1.5$, which has been already reported by Gonçalves several years ago[21]. In this limit, the OP corresponds to the simple ferrimagnetic phase in which both sublattice magnetization are fully saturated and also antiparallel oriented with respect to each other (in fact, $m_A = -0.5$ and $m_B = 1.0$).

The situation becomes much more complicated by turning on the biaxial anisotropy E. Even though the sublattice magnetization m_A remains at its saturation value in the whole OP, the sublattice magnetization m_B is gradually suppressed by increasing the biaxial anisotropy strength. In contrast, neither sublattice magnetization, nor the quadrupolar moment do not depend within either ground state phase on the uniaxial crystal-field potential D. Of course, the relevant change of sublattice magnetization m_B must reflect a violation of a perfect ferrimagnetic spin arrangement in the OP. To achieve the non-saturated m_B at $T = 0$, some spins of sublattice B must flip from the $|+1\rangle$ to $|-1\rangle$ and/or $|0\rangle$ state(s). It is therefore of great importance to identify the magnitude of the quadrupolar moment q_B^z. Since the quadrupolar moment approaches in the OP its saturation value $q_B^z = 1.0$ independently of E/J, a presence of the $|0\rangle$ states can be thus clearly excluded. These observations would suggest, that the biaxial anisotropy causes in the OP a spin tunneling between the $|+1\rangle$ and $|-1\rangle$ states, whereas the stronger the ratio E/J, the greater the population of the $|-1\rangle$ state. Anyway, the probabilities to find the spin-1 atom in the $|\pm 1\rangle$ state are given by these simple expressions: $p(|\pm 1\rangle) = \frac{1 \pm m_B}{2}$. Altogether, the spin configuration referring to the OP at $T = 0$ can be characterized as follows: all spin-1/2 atoms are wholly ordered in their spin *down* positions ($m_A = -0.5$), while the spin-1 atoms occupy with the probability $p(|\pm 1\rangle)$ either the $|+1\rangle$, or $|-1\rangle$ state. It should be also pointed out, that the condition $q_B^y > q_B^x$ is always satisfied when $E > 0$. This inequality between the spatial components of quadrupolar momentum provides a confirmation, that x- and y-axis represent under the assumption $E > 0$ the hard- and medium-axis in the OP.

At last, let us consider the spin ordering within the DP. Interestingly, the DP remains unaltered no matter whether the biaxial anisotropy is zero, or not. Indeed, all spin-1 atoms occupy in the DP exclusively the $|0\rangle$ state, because of $m_B = q_B^z = 0.0$. Contrary to this, the components of quadrupolar moment perpendicular to the z-axis acquire in the DP their maximum value $q_B^x = q_B^y = 1.0$. These results can be thought as an independent check for the scenario that accompanies the phase transition from the OP to DP: all spin-1 atoms indeed tending to align into the $x - y$ plane. Accordingly, the magnetic order is completely destroyed, in fact, the vanishing magnetization m_A implies a state of complete spin randomization at sublattice A. Therefore, the DP does not exhibit any long-range magnetic order even at $T = 0$.

Now, another interesting question arises, namely, whether the spin-1 atoms can fluctuate in the OP between their *allowable* $|\pm 1\rangle$ states. In order to obtain a reliable answer to this question, the time-dependent autocorrelation function (24) will be analysed. In the zero-temperature limit, the dynamical autocorrelation function C^{zz}_{auto} gains after straightforward calculation:

$$C^{zz}_{auto}(t) = \frac{(\frac{3}{2})^2 + (\frac{E}{J})^2 \cos\Big(\frac{2Jt}{\hbar}\sqrt{(\frac{3}{2})^2 + (\frac{E}{J})^2}\Big)}{(\frac{3}{2})^2 + (\frac{E}{J})^2}, \tag{28}$$

which in turn proves that C^{zz}_{auto} is periodic in time with the angular frequency $\omega_u = \frac{2J}{\hbar}\sqrt{(\frac{3}{2})^2 + (\frac{E}{J})^2}$ and the recurrence time $\tau = \frac{\pi\hbar}{J\sqrt{(\frac{3}{2})^2+(\frac{E}{J})^2}}$. According to Eq. (28), the dynamical autocorrelation function does not depend in the ground state on the uniaxial anisotropy D. Owing to this fact, we will further neglect this anisotropy parameter and set $D/J = 0.0$. For illustrative purposes, the time variation of the autocorrelation function C^{zz}_{auto} are displayed in Fig. 3 for several values of the biaxial anisotropy $E/J = 0.1$, 0.5, 1.0 and 2.0. It appears worthwhile to make a few remarks on foregoing results. Since the autocorrelation function varies in time, it clearly demonstrates the zero-temperature spin dynamics between the *allowable* $|\pm 1\rangle$ states. From the analytical solution (28) as well as depicted behaviour one can moreover deduce a physical interpretation of the spin dynamics, namely, the spin system necessarily recovers after the recurrence time τ always its initial state, whereas the stronger the ratio E/J, the shorter the recurrence time τ. In addition, the increasing strength of the biaxial anisotropy enhances also the time-variation of C^{zz}_{auto} (i. e. the amplitude of oscillation). This result is taken to mean, that increasing biaxial anisotropy enlarges also a number of the spin-1 atoms, which tunnel during the recurrence time between the $|\pm 1\rangle$ states. Since the equilibrium magnetization does not varies in time, a number of atoms that tunnel from $|+1\rangle$ to $|-1\rangle$ state, must be definitely the same as a number of atoms that tunnel from the $|-1\rangle$ to $|+1\rangle$ state. These findings have an obvious relevance to the understanding of the zero-temperature spin dynamics, because they enable its explanation from the microscopic viewpoint.

B. Finite-temperature behaviour

In this part, we would like to make some comments on the finite-temperature behaviour of the system under investigation. Let us begin by considering the effect of uniaxial and biaxial anisotropies on the critical behaviour. For this purpose, two typical finite-temperature phase diagrams are illustrated in Fig. 4a and 4b. In both figures, the OP can be located below the phase boundaries depicted as solid lines, while above the relevant phase boundaries the usual paramagnetic phase becomes stable. A closer mathematical analysis reveals, that the temperature-driven phase transition between these two phases is of second-order and belongs to the standard Ising universality class. More specifically, Fig. 4a shows the critical temperature as a function of the uniaxial anisotropy D/J for several values of the biaxial anisotropy E/J. The dependence critical temperature versus uniaxial anisotropy is quite obvious, when increasing D/J, the critical temperature tends monotonically to zero as many as the boundary value (25) is achieved. While the anisotropy term D forces the spins to lie within $x-y$ plane when $D > 0$, the E

term tries to align them into $y-z$ plane. Accordingly, the increasing strength of the biaxial anisotropy supports the magnetic long-range order related to the OP when $D/J > 1.5$ and hence, it survives until stronger anisotropies D/J. As far as the region $D < 0$ is concerned, the biaxial anisotropy substantially lowers the critical temperature of the OP. Apparently, this behaviour arises as a consequence of the fact, that the E term simplifies the transition between the $|\pm 1\rangle$ states due to the non-zero quantum fluctuations. Thus, one can conclude that the quantum fluctuations macroscopically manifest themselves in the reduction of the critical temperature for the easy-axis uniaxial anisotropy (i. e. for $D < 0$, where the model Hamiltonian (1) works extremely well).

To illustrate the influence of the biaxial anisotropy on the critical behaviour, the critical temperature versus biaxial anisotropy dependence is shown in Fig. 4b for several values of the uniaxial anisotropy. As one would expect, the critical temperature gradually decreases with increasing the biaxial anisotropy strength for any $D < 0$. In agreement with the aforementioned arguments, the appropriate depression of the critical temperature can be again attributed to the quantum fluctuations, which become the stronger, the greater the ratio E/J. Apart from this rather trivial finding, one also observes here the interesting dependences with the non-monotonical behaviour of the critical temperature. Namely, for $D/J >> 0.0$ the critical temperature firstly increases and only then gradually decreases with the biaxial anisotropy strength (see for instance the curve for $D/J = 1.3$). To explain such a behaviour, it should be realized that the spin-1 atoms are preferably thermally excited to the $|0\rangle$ state when $D > 0$, what means, that they are preferably excited to the $x-y$ plane. Since the biaxial anisotropy tries to align them into the $y-z$ plane, it favors the long-range order along z-axis in that it prefers the spin tunneling between the $|\pm 1\rangle$ states before the population of the $|0\rangle$ one. The most interesting result to emerge here is that there is a strong evidence, that aforementioned argument explains an existence of the OP even under assumption of extraordinary strong anisotropies $D/J \geq 1.5$. In fact, the magnetic long-range order related to the OP occurs under this condition for the strong enough biaxial anisotropies only. Surprisingly, the magnetic long-range order results in such a peculiar case from the quantum fluctuations (spin tunneling) caused by the biaxial anisotropy.

Now, let us provide an independent check of the critical behaviour by studying the thermal dependences of magnetization. The single-site magnetization against the temperature are plotted in Fig. 5 for the uniaxial anisotropy $D/J = -2.0$ and several values of the biaxial anisotropy E/J. Fig. 5a shows a typical situation observed by turning on the biaxial anisotropy E/J: the greater this anisotropy parameter, the stronger the reduction of sublattice magnetization m_B due to the $|\pm 1\rangle$ spin tunneling. As it is apparent from this figure, the total magnetization exhibits in general the standard Q-type dependences. The most striking thermal variations of the total magnetization can be evidently found for the biaxial anisotropies close to the value $E_c^0/J = \sqrt{27}/2$, at which m_A fully compensates m_B in the ground state (Fig. 5b, see also Fig. 2b). It turns out, however, that all marvellous thermal dependences of the total magnetization stemming from the identical origin - the magnetization of sublattice A is thermally more easily disturbed than the magnetization of sublattice B. As a result, the P-type dependences of total magnetization occur for $E < E_c^0$, when the prevailing magnetization m_B exhibits smaller thermal variation than the lower

magnetization m_A (see cases $E/J = 2.58$ and 2.59 in Fig. 5b). Based on our earlier remark concerning the ground-state properties, $|m_A|$ exceeds m_B if $E > E_c^0$ is satisfied. Then, when the value of biaxial anisotropy is from the vicinity E_c^0, a more rapid thermal variation of m_A results in the N-type dependence with one compensation point. As a matter of fact, the total magnetization shows one compensation point in which spontaneous magnetization reverses its sign, because at lower temperatures $|m_A| > m_B$, while at higher temperatures $|m_A| < m_B$ (see the curve for $E/J = 2.61$). In addition, even for more stronger biaxial anisotropies the R-type dependences of total magnetization appear ($E/J = 2.63$). In such a case, the total magnetization retrieves its substandard slope from the faster thermal variation of always dominating magnetization m_A.

Finally, let us proceed to the discussion of the spin dynamics at non-zero temperatures. The time variations of the autocorrelation function C_{auto}^{zz} are plotted in Fig. 6 for three selected values of biaxial anisotropies $E/J = 0.1$, 0.5 and 2.0. To enable a comparison between the autocorrelation functions at various E/J, the relevant temperatures are normalized with respect to their critical temperatures. It can be easily realized that the autocorrelation function is not in general a periodic function of time at non-zero temperatures. Indeed, C_{auto}^{zz} arises according to Eq. (28) as a superposition of two harmonic oscillations - oscillation with higher angular frequency $\omega_u = \frac{2J}{\hbar}\sqrt{(\frac{3}{2})^2 + (\frac{E}{J})^2}$ and another one with lower angular frequency $\omega_l = \frac{2J}{\hbar}\sqrt{(\frac{1}{2})^2 + (\frac{E}{J})^2}$. The interference between these harmonic oscillations with different frequencies and also various amplitudes gives rise to a rather complex time variation of C_{auto}^{zz}, which is in general aperiodic, displaying nodes and other typical interference effects (see Fig. 6). The dependences drawn in Fig. 6 nicely illustrate also the temperature effect on the spin dynamics. Namely, it follows from these dependences, that as the temperature increases, some amplitudes are suppressed, while another ones become more robust. Obviously, in the high-temperature region that amplitudes become dominant, which coincide to the oscillation with lower angular frequency ω_l (see lower panels in Fig. 6). In contrast, the amplitudes arising from higher frequency oscillation ω_u dominate at lower temperatures (see upper panels in Fig. 6). As far as the influence of biaxial anisotropy is concerned, the stronger the ratio E/J, the smaller the difference between both angular frequencies and hence, the more expressive an interference effect between them. It is worth mentioning that some particular biaxial anisotropies keeping the ratio ω_u/ω_l to be rational, what ensures that the autocorrelation function C_{auto}^{zz} is periodic in time even at $T \neq 0$. In any other case, the C_{auto}^{zz} behaves aperiodically. As a result, in the latter case one can impose at best some characteristic time during that the most of spins engaged in the spin dynamics change their states, as it apparent from Fig. 6 (a1, a2, a3). Although this behaviour is quasi-periodic, its characteristic time cannot be confused with the recurrence time τ of the former ones, in fact, the spin system at biaxial anisotropies giving the irrational ratio ω_u/ω_l never approaches its initial state again.

It should be also stressed, that the uniaxial anisotropy D affects the spin dynamics at $T \neq 0$, as well. To illustrate the case, we have depicted in Fig. 7 the time variations of autocorrelation function at $T/T_c = 1.0$ for various uniaxial anisotropies D/J and the ratio $E/J = 0.5$. Referring to this plot, the influence of $|0\rangle$ states on the spin dynamics can be understood more deeply. It is quite evident, that a number of the $|0\rangle$ states becomes negligible by taking into account the easy-axis anisotropy (e.

g. $D/J = -2.0$, Fig. 7a). Really, the quadrupolar moment q_B^z becomes in this case almost saturated, as it can be seen from the time-dependence of $C_{auto}^{zz}(t)$, since $C_{auto}^{zz}(0) = q_B^z$. Contrary to this, the occupation of $|0\rangle$ states becomes crucial when accounting the easy-plane anisotropy (see for instance Fig. 7d displaying the $D/J = 1.5$ case). From the comparison of Fig. 7a-d one can conclude, that positive (negative) anisotropy term D reinforces the higher (lower) frequency oscillation ω_u (ω_l) and hence, the characteristic time becomes considerably shorter (longer). Naturally, the observed behaviour results from the fact, that the critical temperature gradually falls down as the anisotropy term D/J increases. When increasing the ratio D/J, moreover, the oscillation amplitudes are also suppressed, what means, that a smaller number of spins changes during the characteristic time their spin states. This striking feature clarifies, that the $|0\rangle$ states are not engaged in the spin dynamics so greatly as the $|\pm 1\rangle$ states, or even, they do not contribute to the spin dynamics at all.

IV. CONCLUDING REMARKS

In this article, the exact solution of the mixed spin-1/2 and spin-1 Ising model on honeycomb lattice is presented and discussed in detail. The particular attention has been focused on the effect of uniaxial and biaxial crystal-field potentials acting on the spin-1 atoms. As it has been shown, the presence of the biaxial anisotropy modifies the magnetic behaviour of studied system in a crucial manner. It turns out that already a small amount of the biaxial anisotropy raises a non-trivial spin dynamics and basically influences the thermodynamic properties, as well.

The most interesting finding to emerge here constitutes an exact evidence of the spin tunneling between the $|\pm 1\rangle$ states in the magnetically ordered phase (OP). Macroscopically, the tunneling effect decreases the critical temperature for the easy-axis uniaxial anisotropy ($D < 0$) and also, appreciably depresses the magnetization of spin-1 atoms from its saturation value even in the ground state (see Eq. (26) and Fig. 2b). The reduction of critical temperature, as well as magnetization appears apparently due to the local quantum fluctuations arising from the biaxial anisotropy. On the other hand, the same quantum fluctuations can surprisingly cause an onset of the magnetic long-range order for the extraordinary strong easy-plane anisotropies $D/J > 1.5$. To the best of our knowledge, such a result has not been published in the literature before.

It should be also stressed that there is an interesting correspondence between the model described by the Hamiltonian (1) and a similar Ising model with a local transverse magnetic field Ω acting on the spin-1 atoms only (for a comparison, see Ref.[25]):

$$\hat{\mathcal{H}} = J \sum_{\langle k,j \rangle}^{3N} \hat{S}_k^z \hat{\mu}_j^z + \Omega \sum_{k \in B}^{N} \hat{S}_k^x. \tag{29}$$

However, a similarity between the both Hamiltonians (1) and (29) is not accidental, in fact, when neglecting the uniaxial crystal-field potential D in the Hamiltonian (1), an effective mapping $E \leftrightarrow \Omega$ ensures the equivalence between (1) and (29). Since this mapping is not related to the magnetic structure in any fashion, the appropriate correspondence can be apparently extended to several lattice models. It is

therefore valuable to mention, that the magnetic properties of lattice models with the local transverse field become a subject matter of many other theoretical works during the last few years[26]. Whence, the magnetic behaviour of these systems completely resemble that one of their counterparts with the biaxial crystal-field potential E only.

Finally, let us turn back to the origin of biaxial anisotropy. Uprise of this anisotropy term in the mixed-spin honeycomb lattice is closely associated with at least a small lattice distortion. To simplify the situation, the proposed Hamiltonian (1) accounts the biaxial crystal-field anisotropy, while a difference between exchange interactions within various spatial directions of the honeycomb lattice has been, for simplicity, omitted. Nevertheless, the developed procedure can be generalized in a rather straightforward way also to a model accounting the anisotropic interactions (J_1, J_2, J_3) within the three non-equivalent directions of honeycomb lattice described by the Hamiltonian:

$$\hat{\mathcal{H}} = \sum_{\langle k,j \rangle}^{3N} J_{kj} \hat{S}_k^z \hat{\mu}_j^z + D \sum_{k \in B}^{N} (\hat{S}_k^z)^2 + E \sum_{k \in B}^{N} [(\hat{S}_k^x)^2 - (\hat{S}_k^y)^2], \tag{30}$$

where the nearest-neighbour exchange constant $J_{kj} = J_1$, J_2 or J_3 in dependence on which of the three non-equivalent spatial direction it deals. In addition, the biaxial anisotropy strength can be even considered as an arbitrary function (linear, quadratic, exponential, logarithmic, ...) of the ratio between appropriate interaction parameters: $E = f(J_2/J_1, J_3/J_1)$. Therefore, another interesting question arises, namely, whether the Ising model with biaxial crystal-field anisotropy taken as a function $E = f(J_2/J_1, J_3/J_1)$ can be instable with respect to the spin-Peierls phenomenon. It is quite reasonable to assume, however, that under certain conditions the energy gain from the biaxial crystal-field anisotropy exceeds the elastic energy related to the lattice deformation and hence, the biaxial anisotropy can lead to a spontaneous lattice distortion. To confirm this suggestion, our future work will be directed in this way.

Acknowledgement: We are grateful to Oleg Derzhko and Taras Verkholyak for stimulating discussion and useful suggestions during the Small Triangle Meeting 2003 in Medzev.
This work was supported under the VEGA Grant No. 1/9034/02 and the APVT Grant No. 20-009902.

---

[1] R. Sessoli and D. Gatteschi, Angew. Chem. **42**, 268 (2003).

[2] A. L. Barra, A. Caneschi, A. Cornia, F. Fabrizi de Biani, D. Gatteschi, C. Sangregorio, R. Sessoli and L. Sorace, J. Am. Chem. Soc. **121**, 5302 (1999);
G. Amoretti, S. Carretta, R. Caciuffo, H. Casalta, A. Cornia, M. Affronte, D. Gatteschi, Phys. Rev. B **64**, 104403 (2001).

[3] K. Wieghardt, K. Pohl, I. Jibril, G. Huttner, Angew. Chem. **96**, 63 (1984);
M. Hennion, L. Pardi, I. Mirebeau, E. Suard, R. Sessoli, A. Caneschi, Phys. Rev. B **56**, 8819 (1997);

R. Sessoli, D. Gatteschi, A. Caneschi, M. A. Novak, Nature **365**, 141 (1993);
R. Sessoli, Mol. Cryst. Liq. Cryst. **274**, 145 (1995).

[4] J. C. Goodwin, R. Sessoli, D. Gatteschi, W. Wernsdorfer, A. K. Powell and S. L. Health, J. Chem. Soc. Dalton Trans., 1835 (2000);
M. Affronte, J. C. Lasjaunias, W. Wernsdorfer, R. Sessoli, D. Gatteschi, S. L. Health, A. Fort and A. Rettori, Phys. Rev. B **66**, 064408 (2002).

[5] W. Wernsdorfer, S. Bhaduri, C. Boskovic, G. Christou and D. N. Hendrickson, Phys. Rev. B **65**, 180403 (2002).

[6] J. Oitmaa and A. M. A. von Brasch, Phys. Rev. B **67**, 172402 (2003).

[7] K. K. Pan and Y.-L. Wang, Phys. Rev. B **51**, 3610 (1995).

[8] N. Ch. Eddeqaqi, M. Saber, A. El-Atri and M. Kerouad, Physica A **272**, 144 (1999);
W. Jiang, G. Z. Wei and A. Du, J. Magn. Magn. Mater. **250**, 49 (2002);
W. Jiang, G. Z. Wei, A. Du and L. Q. Guo, Physica A **313**, 503 (2002);
W. Jiang, G. Z. Wei and Q. Zhang, Physica A **329**, 161 (2003).

[9] G. P. Taggart, R. A. Tahir-Kheli and E. Shiles, Physica **75**, 234 (1974);
R. Mienas, Physica A **89**, 431 (1977).

[10] K. K. Pan and Y.-L. Wang, Phys. Lett. A **178**, 325 (1993).

[11] T. Moriya, Phys. Rev. **117**, 635 (1960).

[12] L. Berger and S. A. Friedberg, Phys. Rev. **136**, A158 (1964).

[13] L. G. Polgar and S. A. Friedberg, Phys. Rev. B **6**, 3497 (1972).

[14] H. Kumagai, K. Ôno, I. Hayashi and K. Kambe, Phys. Rev. **2**, 374 (1952).

[15] M. E. Lines, Phys. Rev. **137**, A982 (1965).

[16] N. Uryû, J. Skalyo and S. A. Friedberg, Phys. Rev. **144**, 684 (1966).

[17] G. C. DeFotis, F. Palacio and R. L. Carlin, Phys. Rev. B **20**, 2945 (1979);
G. C. DeFotis, B. K. Failon, F. V. Wells and H. H. Wickman, Phys. Rev. B **29**, 3795 (1984).

[18] Z. J. Zhong, N. Matsumoto, H. Ōkawa, S. Kida, Chem. Lett., 87 (1990);
H. Tamaki, M. Mitsumi, K. Nakamura, N. Matsumoto, S. Kida, H. Ōkawa and S. Iijima, Chem. Lett., 1975 (1992);
H. Tamaki, Z. J. Zhong, N. Matsumoto, S. Kida, M. Koikawa, Y. Aihiwa, Y. Hashimoto and H. Ōkawa, J. Am. Chem. Soc. **114**, 6974 (1992);
S. Iijima, T. Katsura, H. Tamaki, M. Mitsumi, N. Matsumoto and H. Ōkawa, Mol. Cryst. Liq. Cryst. Sci. Technol. A **233**, 263 (1993);
S. Decurtins, S. W. Schmalle, H. R. Ostwald, A. Linden, J. Ensling, P. Gütlich and A. Hauser, Inorg. Chim.

Acta **216**, 65 (1994);
C. Mathonière, S. G. Carling, Y. Dou and P. Day, J. Chem. Soc. Chem. Commun., 1554 (1994);
W. M. Reiff, J. Kreisz, L. Meda and R. U. Kirss, Mol. Cryst. Liq. Cryst. Sci. Technol. A **273**, 181 (1995);
C. Mathonière, C. J. Nuttall, S. G. Carling and P. Day, Inorg. Chem. **35**, 1201 (1996).

[19] T. Kaneyoshi, Y. Nakamura and S. Shin, J. Phys.: Condens. Matter **10**, 7025 (1998);
Y. Nakamura, J. Phys.: Condens. Matter **12**, 4067 (2000);
Y. Nakamura, Phys. Rev. B **62**, 11742 (2000);
Y. Nakamura, Prog. Theor. Phys. **138**, 466 (2000);
G. M. Buendia and E. Machado, J. Magn. Magn. Mater. (2004).

[20] J. Strečka, M. Jaščur, Acta Electrotechnica et Informatica **2**, 102 (2002) (cond-mat/0207519).

[21] L. L. Gonçalves, Physica Scripta **32**, 248 (1985);
L. L. Gonçalves, Physica Scripta **33**, 192 (1986);
J. W. Tucker, J. Magn. Magn. Mater. **95**, 133 (1999).

[22] R. B. Potts, Phys. Rev. **88**, 352 (1952);
G. F. Newell, Phys. Rev. **79**, 876 (1950);
R. M. F. Houtappel, Physica **16**, 425 (1950);
H. N. V. Temperley, Proc. Roy. Soc. **203A**, 202 (1950);
R. J. Baxter and T. Choy, Proc. Roy. Soc. London Ser. A **423**, 279 (1989);
J. H. Barry, T. Tanaka, M. Khatun and C. H. Múnera, Phys. Rev. B **44**, 2595 (1991).

[23] E. Balcar, S. W. Lovesey, *Theory of magnetic neutron and photon scattering*, (Clarendon, Oxford, 1989).

[24] T. Moriya, Prog. Theor. Phys. **16**, 23 (1956).

[25] M. Jaščur, S. Lacková, J. Phys.: Condens. Matter **12**, L583 (2000).

[26] M. Jaščur, J. Strečka, Phys. Lett. A **258**, 47 (1999);
J. Strečka, H. Čenčariková, M. Jaščur,
Acta Electrotechnica et Informatica **2**, 107 (2002) (cond-mat/0207518);
H. Suzuki, M. Suzuki, Int. J. Mod. Phys. B **16**, 3871 (2002);
J. Strečka, M. Jaščur, J. Magn. Magn. Mater. **260**, 415 (2003);
Y. Fukumoto and A. Oguchi, J. Magn. Magn. Mater. (2004).

Figure captions

Fig. 1 The segment of a mixed-spin honeycomb lattice. The lattice positions of the spin-1/2 (spin-1) atoms are schematically designated by full (open) circles, the solid lines label the interactions between nearest-neighbouring atoms. The dashed lines represent the effective interaction between three outer spin-1/2 atoms, which arise after performing the mapping (9) at kth site.

Fig. 2 a) Ground-state phase diagram in the $E/J - D/J$ plane; b) Single-site magnetizations (full lines) and quadrupolar moment (broken ones) versus the biaxial anisotropy E/J at $T = 0$ and $D/J = 0.0$.

Fig. 3 Time variation of the dynamical autocorrelation function C^{zz}_{auto} for various values of biaxial anisotropies $E/J = 0.1$, 0.5, 1.0 and 2.0. Time axis is scaled in $\hbar/J$ units.

Fig. 4 a) Critical temperature dependence on the uniaxial anisotropy D/J for several values of biaxial anisotropies E/J; b) Critical temperature dependence on the biaxial anisotropy E/J for several values of uniaxial anisotropies D/J.

Fig. 5 a) Thermal dependences of the total and sublattice single-site magnetization for $D/J = -2.0$ and $E/J = 0.0$, 1.0 and 2.0; b) Various temperature dependences of the total magnetization normalized per one site when the strength of uniaxial anisotropy is fixed ($D/J = -2.0$) and the biaxial anisotropy varies in the vicinity of E^0_c.

Fig. 6 Time variations of the dynamical autocorrelation function C^{zz}_{auto} when $D/J = 0.0$ is fixed and $E/J = 0.1$, 0.5 or 2.0. Upper, central and lower panels show the time variation of C^{zz}_{auto} at three various temperatures, which are normalized with respect to their critical temperatures to ensure the same ratio $T/T_c = 0.8$, 1.0 and 1.1, respectively.

Fig. 7 The time variations of dynamical autocorrelation function C^{zz}_{auto} at critical temperature ($T/T_c = 1.0$), $E/J = 0.5$ and several values $D/J = -2.0$, 1.0, 1.3 and 1.5.

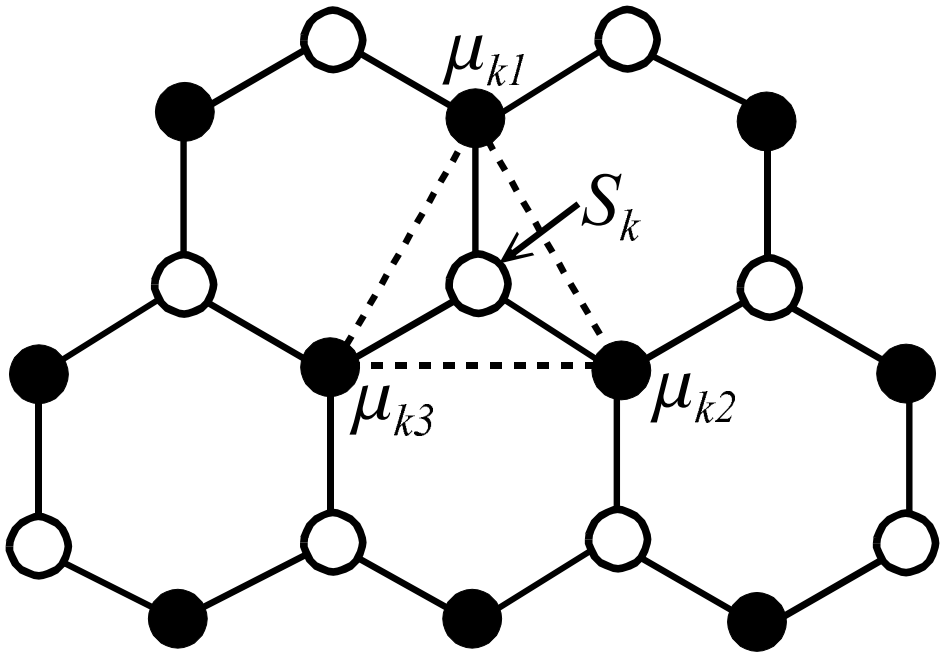

Fig. 1 Strecka et al.

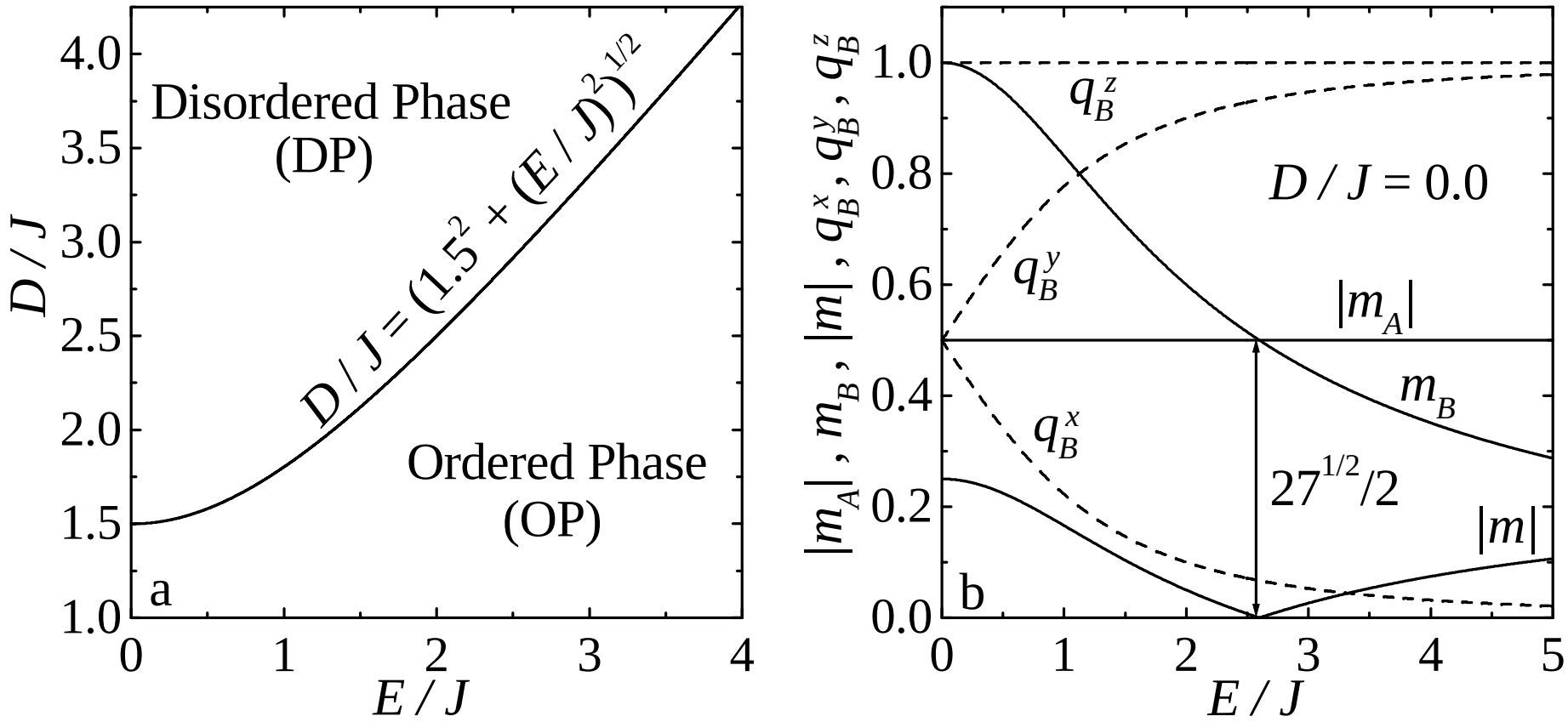

Fig. 2 Strecka et al

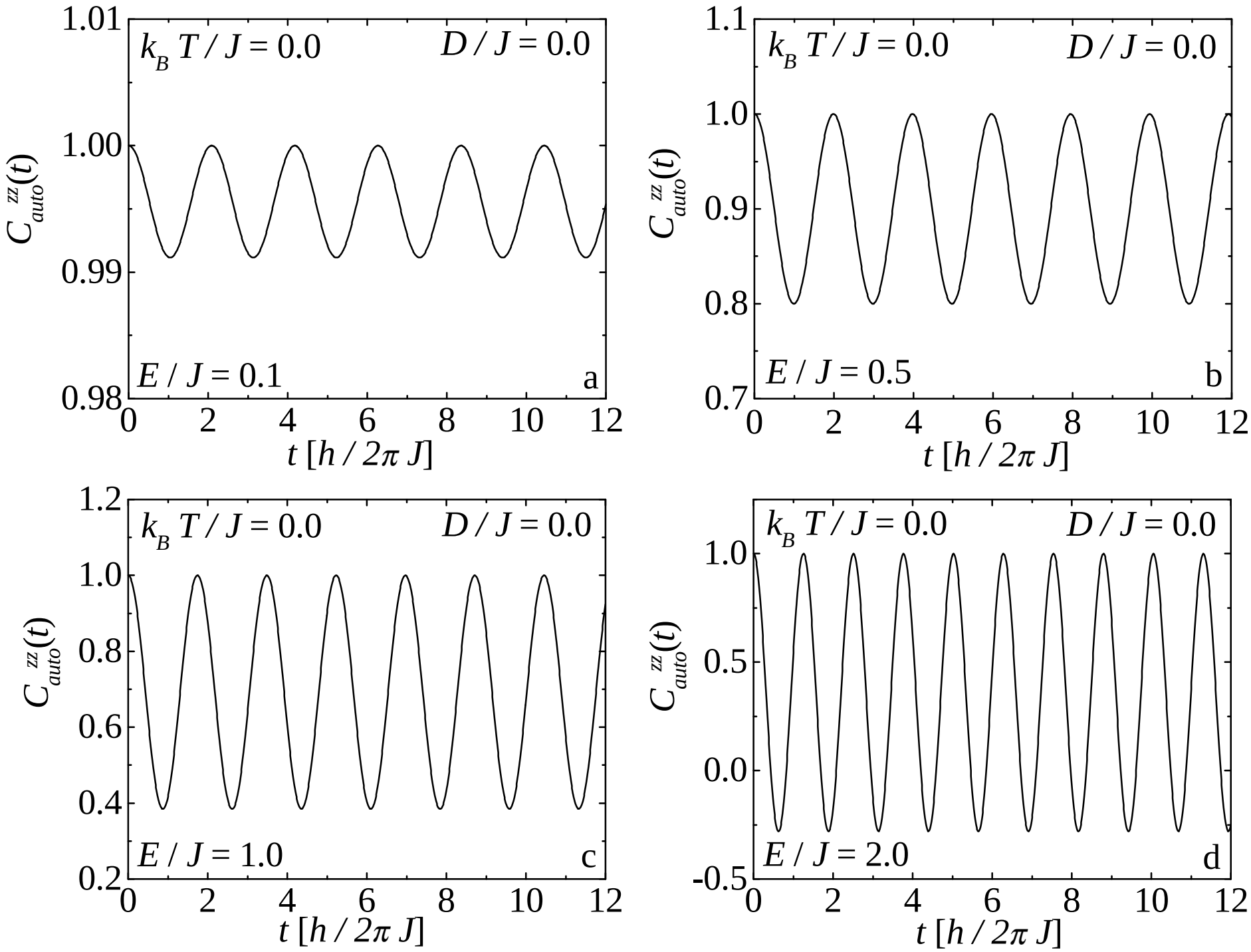

Fig. 3 Strecka et al.

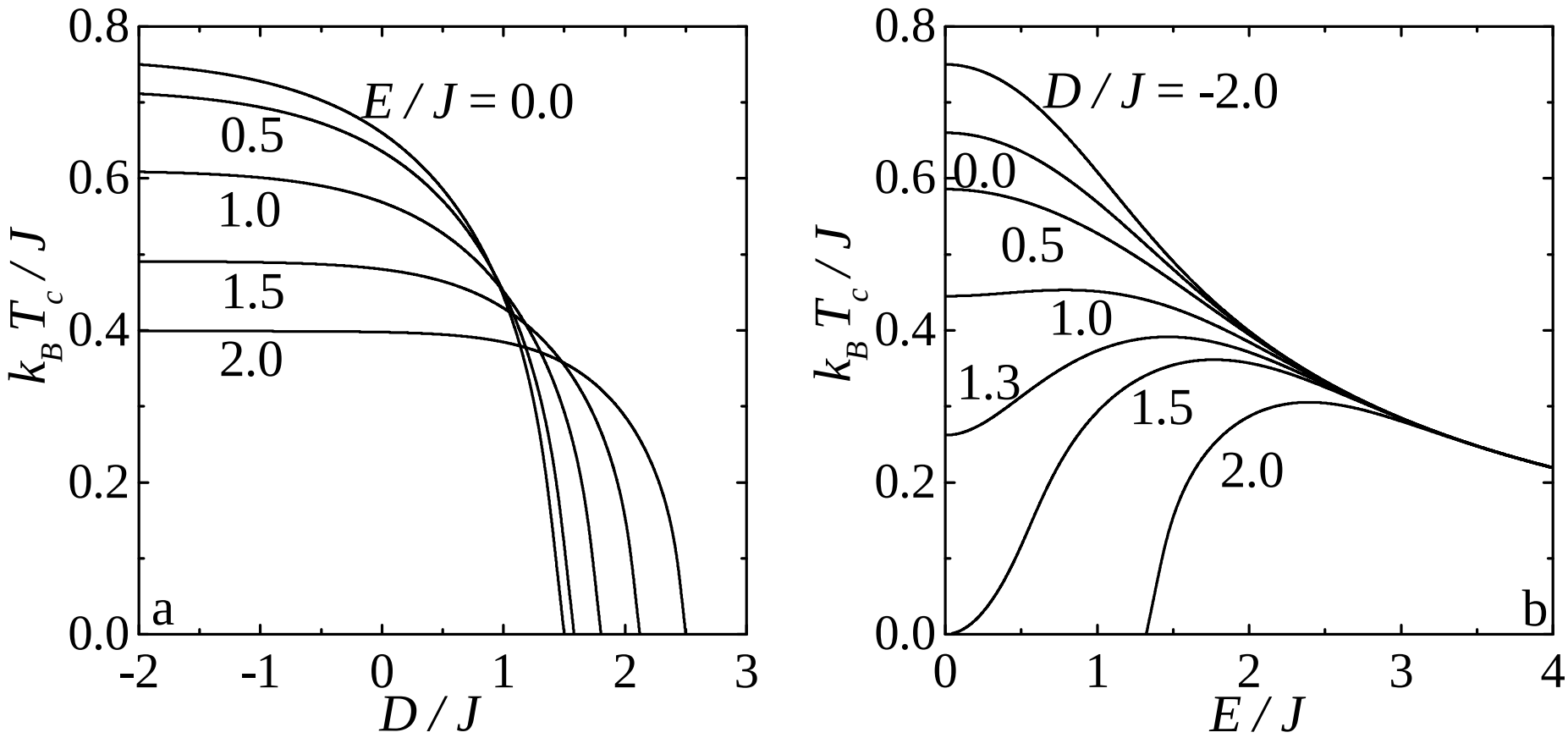

Fig. 4 Strecka et al.

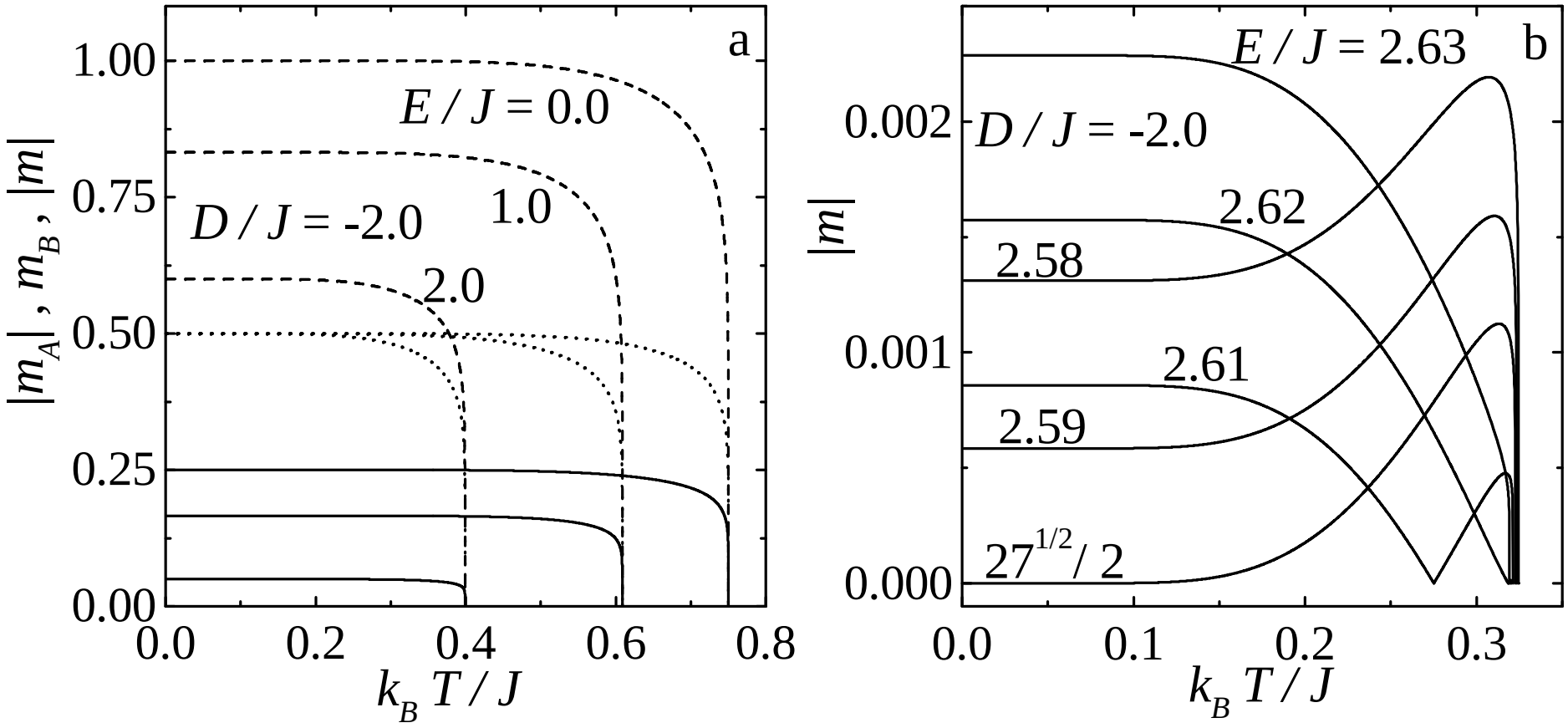

Fig. 5 Strecka et al.

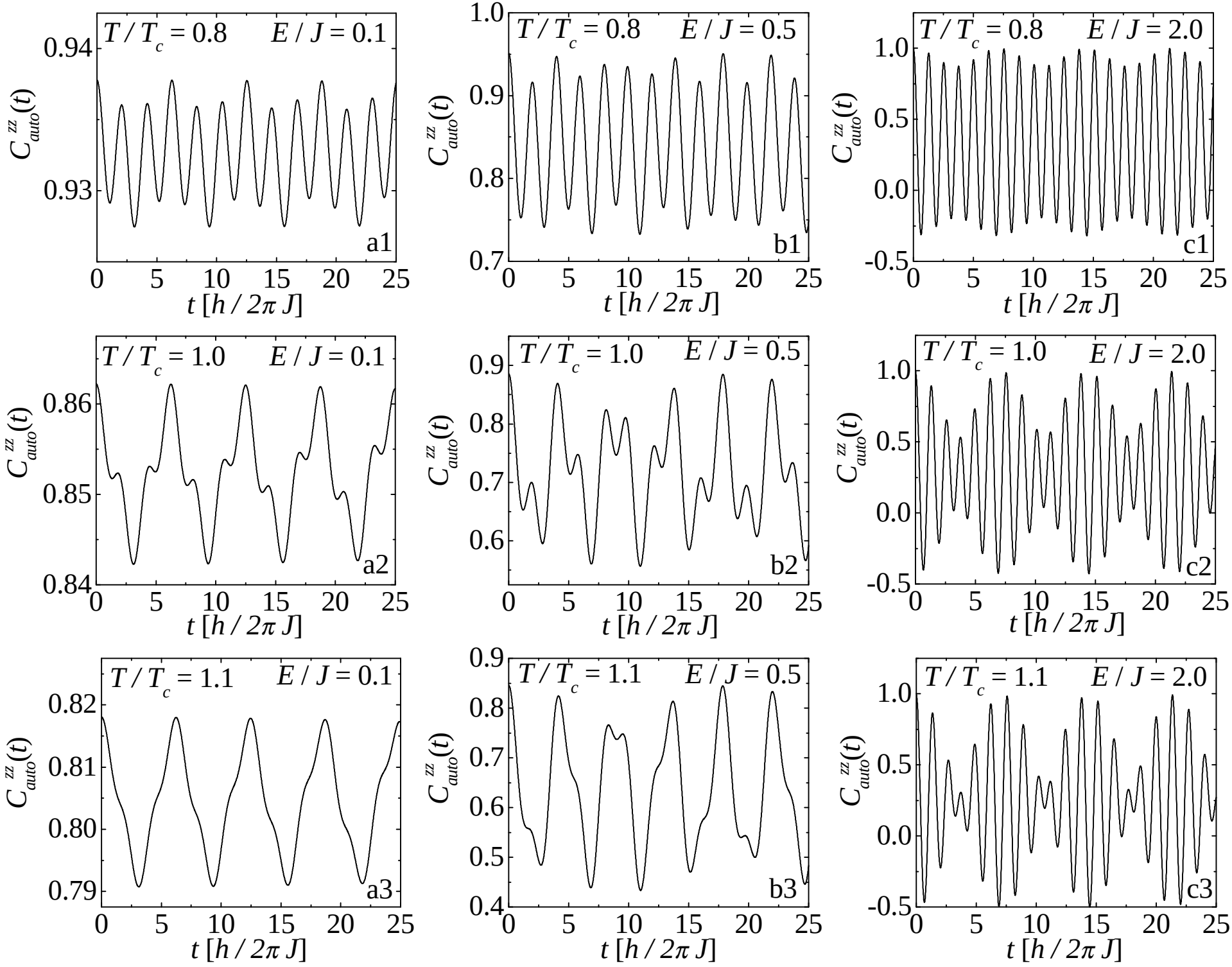

Fig. 6 Strecka et al.

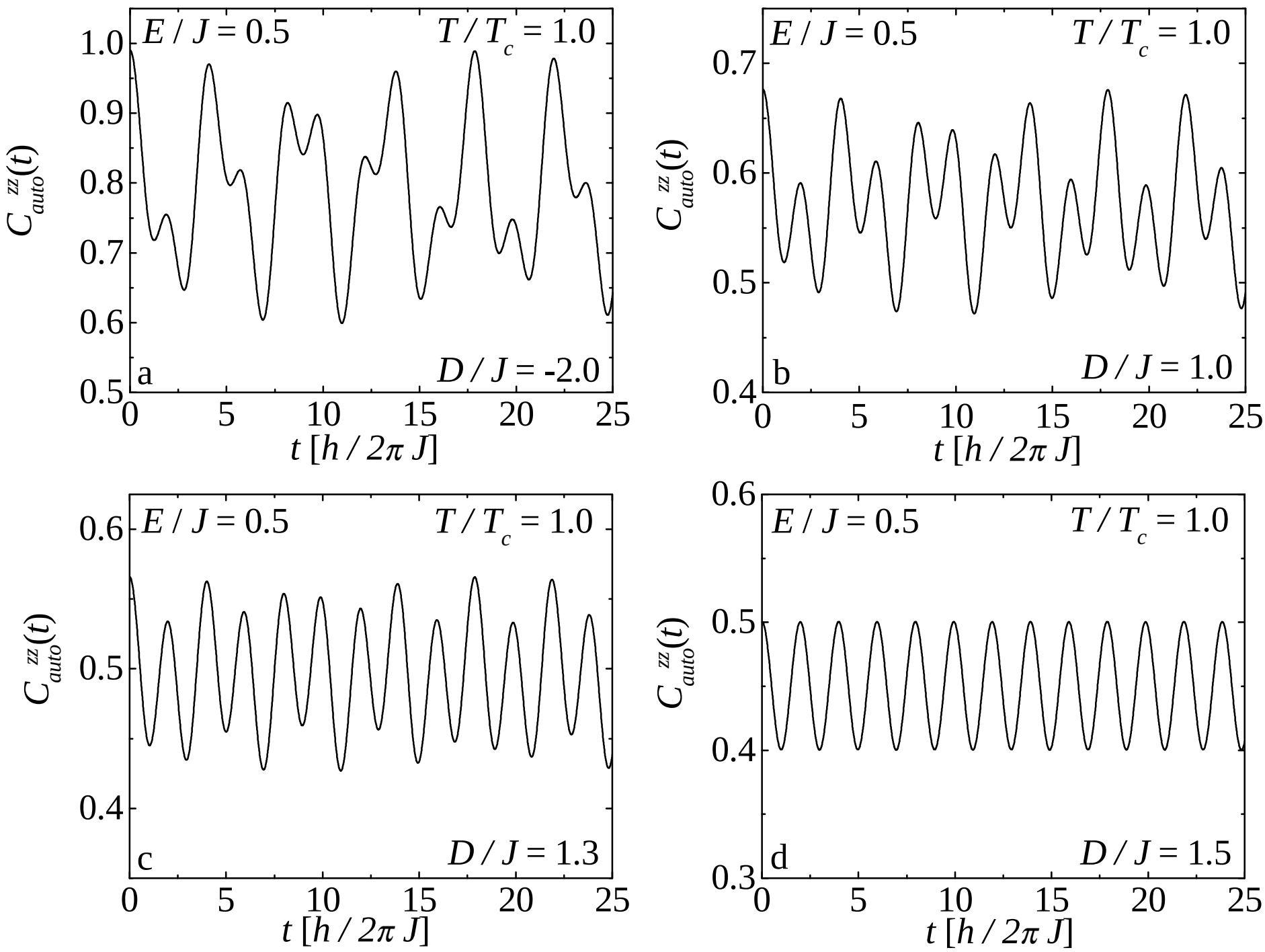

Fig. 7 Strecka et al.